On the use of modal works of cutting forces to optimize machining conditions in the presence of vibrations

Marc Raffestin[a,b], Mikhaïl Guskov[a], Philippe Lorong[a,*], Cyrille Urville[b]

[a] *Laboratoire PIMM, Arts et Metiers Institute of Technology, CNRS, Cnam, HESAM Universite, 151 boulevard de l'Hopital, Paris, 75013, France*
[b] *PCI SCEMM, Rue Copernic, Saint-Etienne, 42030, France*

Abstract

The use of Virtual Machining models may be a valuable approach in the designing stage of a machining operation as long as the models are sufficiently accurate. When vibration risks are suspected, stability analysis approaches to predict regenerative chatter phenomena are generally used. However, although these approaches, when applicable, allow efficient numerical optimization of the process around an operating point, they often require other strong assumptions such as neglecting transient phenomena or oversimplifying kinematics. On the other hand, time domain approaches with detailed matter removal modelling allow to monitor the continuous evolution of cutting conditions and represent various phenomena that the models can reproduce (regenerative chatter, forced vibrations, non-linear behaviours). The amount of data produced is, however, considerable and often costly to analyse. It may therefore be interesting to deduce, from these data, scalar indicators allowing

*Corresponding author
Email addresses: marc.raffestinpro@laposte.net (Marc Raffestin), mikhail.guskov@ensam.eu (Mikhaïl Guskov), philippe.lorong@ensam.eu (Philippe Lorong), cyrille.urville@pci.fr (Cyrille Urville)

easier and more relevant analysis of the simulation results.
In this work, the modal work of the cutting forces upon the workpiece vibratory displacements is proposed as an indicator to discriminate different tool paths. A one degree of freedom theoretical problem and a face milling operation on extruded aluminum profiles extracted from automotive structural part are used to explain and show the relevance of such indicator.
Keywords: machining, flexible part, flexible tool, cutting forces, vibrations, time domain simulations, modal works

---

1. Introduction

In automotive industry, the transition from internal combustion engine to electric vehicles is accompanied by the appearance of new structural parts which may be difficult to machine. This is, for example, the case of the battery trays which are made up of several extruded aluminium sections assembled together. For these lightweight structure components, dynamic effects, or part deflexion under cutting forces or clamping, can be significant during machining. The static or dynamic flexibility of these parts is then a major factor in the evaluation of their machinability. Indeed, when vibrations occur, the acceptability of a machining operation is not only related to the quality of obtained geometry of the machined surface. The perturbation induced on the cutting forces evolution (applied on each individual tooth) must also remain small with respect to the expected one without vibration. The expected level for this acceptability remains a choice of the end user and it is important, from the very first stages of designing production resources, to choose cutting conditions that enable the expected part quality to be

obtained. Numerical simulations, based on a virtual model of the machining operation, is then a useful mean for determining vibratory behaviour of the part/machine/tool system.

Effects induced by the lack of stiffness during machining, such as chatter or forced vibrations, are well known and the classical way to evaluate machinability in presence of vibration is to use stability analysis [1, 2]. Several solutions to ensure part quality in this case are present in the literature [3]. The tool path is one of the factors influencing the stability of machining. In particular, the difference between conventional and climb milling on dynamic behaviour of a machining operation if studied in [4, 5] and an optimization of machining strategy enabling to limit dynamic deflection under cutting forces for multiple paths operations is proposed in [6]. In-process workpiece monitoring of the part deflection for detection of chatter occurrence can also be used to optimize tool path [7, 8, 9]. Experimental approaches enable this detection in real time allowing immediate corrective action [10, 11].

Although stability analysis approach is often a good way to prevent chatter occurence it does not provide information on the complete progress of a machining operation (history of cutting forces and vibrations for example) and would not allow the study of transient behaviors, frequent when the part or the tool trajectory are complex. Such phenomena can however be predicted thanks to time domain simulations [12, 13, 14, 15]. Although the latter make it easier to take into account non-linear phenomena involved in the machining process, they are nevertheless significantly more costly in terms of calculation time. Moreover, when using time domain approach it is not straightforward to use produced raw digital data to estimate machining

acceptability. The post-processing of these data is then an important aspect for their analysis and their exploitation by user. In the presence of vibrations, it is interesting to extract information making it possible to differentiate the contribution and the relative importance of the various eigenmodes of the system to counter these vibrations.

The present paper deals with the use of energetic indicators, extracted from a time domain simulation, to help a user to optimize machining conditions when vibration may occur. More precisely, modal works generated by cutting forces will be used as indicator to compare the acceptability of different tool path cases and to analyse the evolution of the contribution of each individual eigenmode during different machining conditions. This indicator is cheap to compute and directly deduced from raw data obtained via a numerical time domain approach which bases its dynamic modelling on a set of eigenmodes (for the tool and/or the part). With this indicator the user has, for each mode of the machining system, the evolution of a scalar quantity whose amplitude allows to appreciate the energy introduced into the corresponding mode. The raw simulation data contains, for its part, the cutting forces produced by each individual tooth and applied on a part whose vibration amplitude (deduced from the contribution of all eigenmodes) depends on the location where each of these forces is applied. The definition of the indicator is inspired by the work of G. Vermot des Roches and E. Balmes [16] (section 2.3.2) who use the mechanical energy of a system as an indicator to study damping effects. In the field of machining, energetic approach is already used to handle part distorsion induced by the presence of initial residual stress prior to machining [7, 17].

We begin, in section 2, by defining the proposed indicator and by giving the way the modal works of cutting forces are computed. We then propose, section 3, a first study of its behaviour for a system with only one degree of freedom. A quite more complex application on a real machining operation is detailed in section 4. This application needs to use a specific software, the *nessy2m* developed within the PIMM laboratory, to offer a more realistic machining modelling, involving superposition of multiple eigenmodes issued from Finite Element (FE) modal analysis, alongside discretized matter removal process representation. Finally, before concluding in section 6, we propose, in section 5, an analysis of the contribution of this indicator to reproduce experimental trends and of its ability to discriminate between trajectories.

2. Modal works definition

We focus here on the part because it often is, particularly for thin-walled parts, the weak component of the machine/tool system. Before projection on a chosen eigenmodes basis, the equation of motion of the part is set in a finite element (FE) framework and can be written as follows:

$$\underline{\underline{M}}\,\underline{\ddot{q}} + \underline{\underline{C}}\,\underline{\dot{q}} + \underline{\underline{K}}\,\underline{q} = \underline{G_c} + \underline{G_o} \tag{1}$$

where $\underline{\ddot{q}}$, $\underline{\dot{q}}$ and $\underline{q}$ are respectively the columns containing accelerations, velocities and displacements of the n_q degrees of freedom of the FE model, $\underline{\underline{M}}$, $\underline{\underline{C}}$ and $\underline{\underline{K}}$ are the corresponding mass, damping and stiffness matrices respectively, $\underline{G_c}$ is the column of FE generalized forces coming from cutting forces exclusively, and finally $\underline{G_o}$ the column of other FE generalized forces

(clamping, inertial effects, ...). We are considering here the case where the amount of material removed during machining is small compared to the volume of the part. It is then possible to consider the matrices $\underline{\underline{M}}$, $\underline{\underline{C}}$ and $\underline{\underline{K}}$ as constants. Nevertheless, when the impact of material removal on the dynamic behaviour of the part can no longer be neglected, a strategy to take into account its evolution must be implemented.

At a given point A of the part, and at a given time t, the FE interpolation defines the displacement $\underline{U}(A,t)$ and the velocity $\underline{V}(A,t)$, both columns of 3 components inside the global FE frame, by:

$$\underline{U}(A,t) = \underline{\underline{N}}(A)\,\underline{q}(t), \quad \underline{V}(A,t) = \underline{\underline{N}}(A)\,\underline{\dot{q}}(t) \tag{2}$$

where $\underline{\underline{N}}(A)$ is the matrix of global FE shape functions whose size is $3 \times n_q$.

To model cutting forces, as will be specified later (section 4.2), a discretization of each rake face is done and produces a set of elementary tools. When an elementary tool k cuts matter, a cutting force is computed. The column ${}^k\underline{F}$ of its 3 components is:

$${}^k\underline{F} = {}^kb\,\left(F_n({}^kh)\,{}^k\underline{n} + F_e({}^kh)\,{}^k\underline{e} + F_c({}^kh)\,{}^k\underline{c}\right) \tag{3}$$

where ${}^kb$ and ${}^kh$ are the cut width and the cut chip thickness of elementary tool k respectively, $({}^k\underline{n}, {}^k\underline{e}, {}^k\underline{c})$ the column of component of the basis $({}^k\mathbf{n}, {}^k\mathbf{e}, {}^k\mathbf{c})$ of the elementary tool k inside the global FE frame.

The column of FE generalized cutting forces $\underline{G_c}$ is then defined by:

$$\underline{G_c} = \sum_{k=1}^{n_{ET}} \underline{\underline{N}}({}^kA)\;{}^k\underline{F} \tag{4}$$

where n_{ET} is the number elementary tools and ${}^kA$ the point of the part where cutting force is applied.

For parts of complex shapes, the number of degrees of freedom n_q can reach several hundreds of thousands, or even more. In order minimize computation durations, *nessy2m* uses model reduction approach done by a projection inside an eigenmodes Ritz basis. This very classic approach is particularly suitable when one is interested in the vibrations of a mechanical system.

Let $\underline{\underline{\phi}} = [\underline{\phi}_1 \, \underline{\phi}_2 \ldots \underline{\phi}_{n\alpha}]$ be the matrix containing the chosen $n\alpha$ eigenmodes. The number $n\alpha$ is generally of the order of ten or a few tens. The approximation of $\underline{q}$ and $\underline{\dot{q}}$ are then defined by:

$$\underline{q}(t) \approx \underline{\underline{\phi}} \, \underline{\alpha}(t) \quad \text{and} \quad \underline{\dot{q}}(t) \approx \underline{\underline{\phi}} \, \underline{\dot{\alpha}}(t) \tag{5}$$

where $\underline{\alpha}$ is the column of modal degrees of freedom and $\underline{\dot{\alpha}}$ its first derivative with respect to time. The equation of motion in the Ritz basis can then be written as follows:

$$\underline{\underline{m}} \, \underline{\ddot{\alpha}} + \underline{\underline{c}} \, \underline{\dot{\alpha}} + \underline{\underline{k}} \, \underline{\alpha} \; = \underline{g}_c + \underline{g}_o \tag{6}$$

with $\underline{\underline{m}} = \underline{\underline{\phi}}^T \underline{\underline{M}} \, \underline{\underline{\phi}}$, $\underline{\underline{c}} = \underline{\underline{\phi}}^T \underline{\underline{C}} \, \underline{\underline{\phi}}$ and $\underline{\underline{k}} = \underline{\underline{\phi}}^T \underline{\underline{K}} \, \underline{\underline{\phi}}$ modal mass, damping and stiffness matrices respectively. The column $\underline{g}_c$ contains the modal forces coming from generalized cutting forces $\underline{G}_c$, $\underline{g}_c = \underline{\underline{\phi}}^T \underline{G}_c$ and $\underline{g}_o = \underline{\underline{\phi}}^T \underline{G}_o$ generalized forces coming from other external forces. The column $\underline{g}_c$ is the main driver of part vibrations. It is calculated at the end of each time step of the time marching scheme.

At each time step t, it is possible to compute the power P_c generated by the cutting forces during the motion of the part by:

$$P_c(t) = \sum_{k=1}^{n_{ET}} \underline{V}^T({}^k A, t) \; {}^k\underline{F}(t). \tag{7}$$

By using equations (2), (4) and (5) it is easy to deduce that:

$$P_c(t) = \underline{\dot{\alpha}}^T(t)\ \underline{g}_c(t) = \sum_{i=1}^{n\alpha} \dot{\alpha}_i(t)\, g_{ci}(t). \tag{8}$$

The power P_c is thus the sum, at each time step, of the contributions, for each eigenmode i, of the modal power of cutting force $P_{ci} = \dot{\alpha}_i\, g_{ci}$. No sum on the elementary tools is carried out because g_{ci} are already evaluated within the time marching scheme. This enables to keep relatively low both: *i)* the data to be stored at the end of the simulation (some simulations include several million time steps with several hundred elementary tools), *ii)* the calculation costs.

Finally the work generated by the cutting forces during the part motion for a given time interval T, which in the present work corresponds to a tool revolution, can be computed as follows:

$$W_c(t,T) = \int_t^{t+T} P_c(\tau)\ \mathrm{d}\tau = \sum_{i=1}^{n\alpha} W_{ci}(t,T) \tag{9}$$

where $W_{ci}(t,T) = \int_t^{t+T} P_{ci}(\tau)\ \mathrm{d}\tau$ is the modal work of the cutting forces applied to the part during the time interval $[t,\, t+T]$ on the i^{th} eigenmode.

The maximum value of this modal work can be considered to obtain a scalar descriptor for entire trajectories, enabling for comparisons.

The same treatment can be applied on tool dynamic quantities. The modal works of cutting forces are then expressed within the rotating basis linked to the tool and its eigenmodes are used to compute them. It is important to note that the work calculation (9) does not take into account the displacements induced by the rotation of the spindle: only the modal

displacements are accounted for. Thus the calculated energy corresponds to energy put inside vibrations and does not include the energy consumed by the cutting of material.

This framework enables considering deformable workpiece-machine-tool system in machining-related elastodynamics, suitable for representing distributed deformed shapes and interactions. Thus, a more general scope is addressed than the classical literature references on cutting vibrations, involving lumped parameters models [1, 2]. In the next section we show the link between the modal work concept and usual representation on a one degree-of-freedom (1DOF) delayed oscillator which is a restrictive case of a continuously deformable workpiece-machine-tool system with a detailed surface removal modelling.

3. Illustration on a 1 DOF system

In order to have a first illustration of the behaviour of the proposed descriptor we consider here a delayed forced oscillator, representing a machining case with intermittent tool engagement, corresponding to a system from [2], Fig. 4(b):

$$\ddot{q} + 2\zeta\omega_n\dot{q} + \omega_n^2 q = F \tag{10}$$

with q system's generalized displacement (DOF), ζ damping ratio, ω_n eigenfrequency, F cutting interaction force. The latter is composed as follows:

$$F = g(t)\ \left(\kappa\left(q_T - q\right) + F_0 + F_{\mathrm{pl}}\right), \tag{11}$$

where $q_T = q(t-T)$ is the delayed value of q, $T = \frac{2\pi}{\omega}$ is tool engagement cycle period, equal to the time delay, with ω rotation angular rate,

$$g(t) = \begin{cases} 1 & \text{if mod}\left(\frac{t}{T}, 1\right) < \frac{1}{2} \\ 0 & \text{else} \end{cases}$$

switching function representing intermittent cut (half-period duty cycle in Corpus article's terms), κ apparent cutting stiffness, F_0, F_{pl} additional force terms described below. The two last force terms are added to model finite magnitude response and do not affect the stability boundaries for this system, which are presented on Fig. 1a). F_0 constant nominal cutting force value in absence of vibration, F_{pl} is a ploughing force term:

$$F_{\text{pl}} = \begin{cases} -C_{\text{pl}}\left(\dot{q} - v_0\right) & \text{if } \dot{q} > v_0 \\ 0 & \text{else} \end{cases}.$$

In the present example we consider a time domain simulation for system (10) response in a time span $0 < t < t_{\text{fin}}$. During the simulation time system's parameters are constant except for the cut stiffness κ which varies linearly with time: $\kappa = \kappa_0 \frac{t}{t_{\text{fin}}}$. Numerical parameters used for the simulation are given in Tab. 1, and the resulting system's response $q(t)$ is presented on Fig. 1b).

ω_n	ζ	ω	v_0	C_{pl}	F_0	κ_0	t_{fin}
1	0.05	2.2	0.5	2	1	1	2000

Table 1: 1DOF example simulation parameters

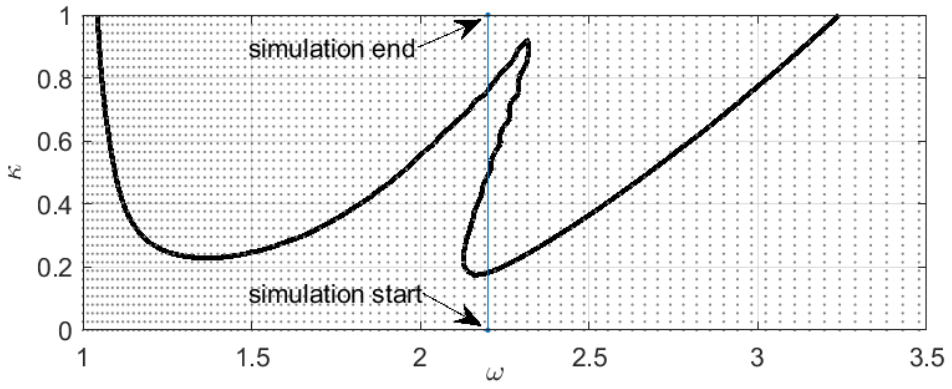

(a) Stability boundaries for 1DOF system, issued from time domain tests. (dots – test points grid, thick line – stability boundary, thin line – simulation trajectory at $\omega = 2.2$)

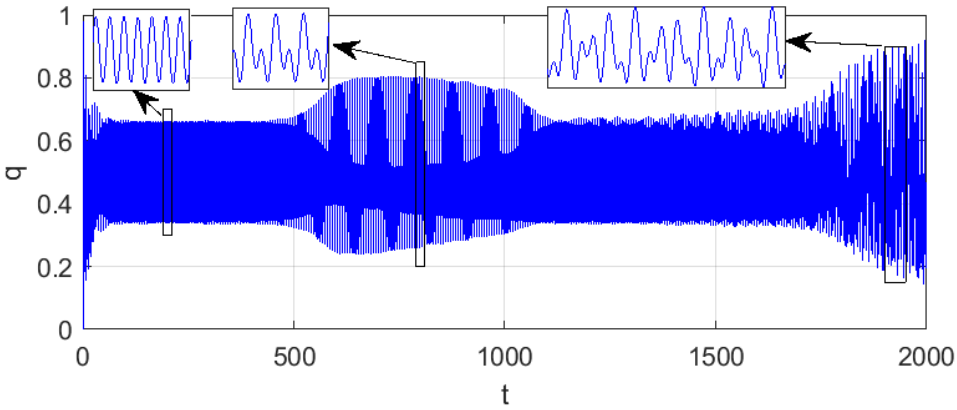

(b) Time series of a solution of (10) at conditions from Tab. 1.

Figure 1: 1 DOF example. Simulation conditions

For this elementary 1DOF case, the kinematics of elastodynamical system can be represented by one single reference point A, for which the velocity is directly equal to the rate of the DOF q, and giving, in relation with the previous section (Eq. (5)):

$$N = 1, \quad \phi = 1, \quad V_A = \dot{q} = \dot{\alpha}, \quad g_c = F, \tag{12}$$

and thus the (9) expression of modal work W_c would reduce to

$$W_c(t,T) = \int_t^{t+T} \dot{q}F \, \mathrm{d}\tau. \tag{13}$$

Fig. 2a) shows this quantity for our simulated response from Fig. 1b). The use of the tool engagement period T for the work calculation (13) renders the W_c smooth in the stable domain (approx. $t < 400$), and the quadratic nature of the work quantity (product of kinematics and force response) provides enhanced readability when a change in vibrational behaviour occurs, as on can see from the comparison of Fig. 1b) and 2a).

Modal work can give place to further analyses, such as Poincaré section. Fig. 2b) , thus visualizing a period-doubling bifurcation in the first vibrations burst.

4. Industrial case

In this section we present an application of modal works to a simulation representing a real case of machining. The considered operation is a face milling of a thin-walled part extracted from industrial battery tray extruded profile component. In order to illustrate the benefits of the indicator, two different machining trajectories are studied: one leading to vibration occurrence and the other not. We begin by presenting this case (section 4.1). The simulation of the latter requires a complex modelling that is introduced in the *nessy2m* software. After briefly describing this software section 4.2 we give, section 4.3, the main particularities of the modelling of the machining operation considered. Finally, before studying the obtained temporal evolutions of cutting modal works in section 4.6, we firstly compare, in section 4.4,

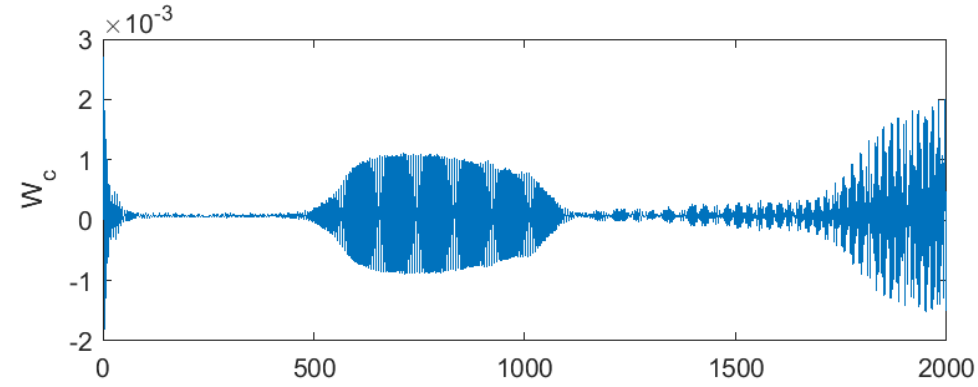

(a) $W_c(t, T)$

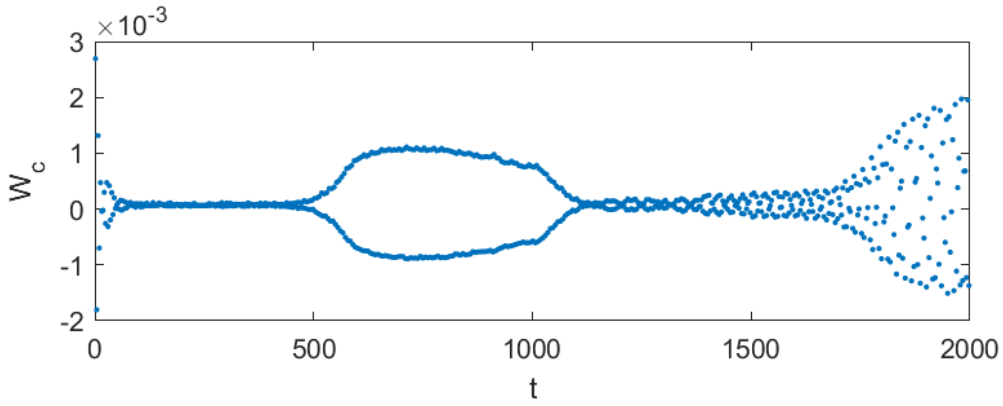

(b) $W_c(t, T)$ sampled with T period

Figure 2: Modal work for 1 DOF illustration.

virtual machining to real machining. One of the objectives is to verify that the simulation is sufficiently representative to allow relevant discrimination of the two trajectories. We then secondly study, in section 4.5, the raw data obtained by simulation (cutting forces and vibration). The latter analysis is facilitated by the fact that, at a given moment, only one tooth is engaged with the material.

4.1. Machining operation description

The part under consideration is a battery tray element, constituted by an extruded aluminium 6060 T6 profile piece of size (XYZ) $75 \times 400 \times 110$ (mm) (Fig. 3). Its thin-walled shape makes it subject to vibration during machining. The section of the part, normal to the extrusion direction $\mathbf{Y}$, is visible on Fig. 4.

Figure 3: Part in machining center with impact hammer

The part is held by screwed clamps (Norelem ref 04371), tightened at 9 N.m on supports (Norelem ref 02040). The supports are located at 120 mm

(**Y** direction) from the part sides and 5 mm from the lateral sides (**X** direction).

A face milling operation is considered Fig. 4. The tool path is a simple translation along the **Y** direction. The cutter is an insert mill (MAPAL ref. 30545058, overhang $L = 110\,\text{mm}$, diameter $D = 80\,\text{mm}$, with $Z = 10$ inserts ref. 30559594) with constant feed rate of $f = 0.05\,\text{mm/tooth}$, cutting depth $a_p = 1\,\text{mm}$ (in **Z** direction) and rotation speed of $N = 18\,000$ rev/min. These cutting conditions correspond to an industrial use case.

An accelerometer is placed, during machining and hammer testing, on the base of the part. It localisation is shown in Fig. 4a and Fig. 5. Accelerations are measured in **Z** direction. Such sensor placement offers a trade-off between the excessively high vibration levels in the vicinity of cutting zone, and excessively low vibrations on the clamping zone. These vibration measurements are completed with metrology of the machined surface, providing an a posteriori insight into the relevance of the simulation model.

The distance d in direction **Z**, see Fig. 4a, between the tool axis and the symmetry plane $(\mathbf{Y}, \mathbf{Z})$ of the part is a design parameter.

4.2. General time domain approach

For the current application the used time domain solver is implemented inside the *nessy2m* software. The reader will find more details on the foundations of *nessy2m* in the internal report [18].

nessy2m requires as inputs:

- A geometrical model of the machined surface: this model is used to follow the erasing of material by the teeth during each time step in

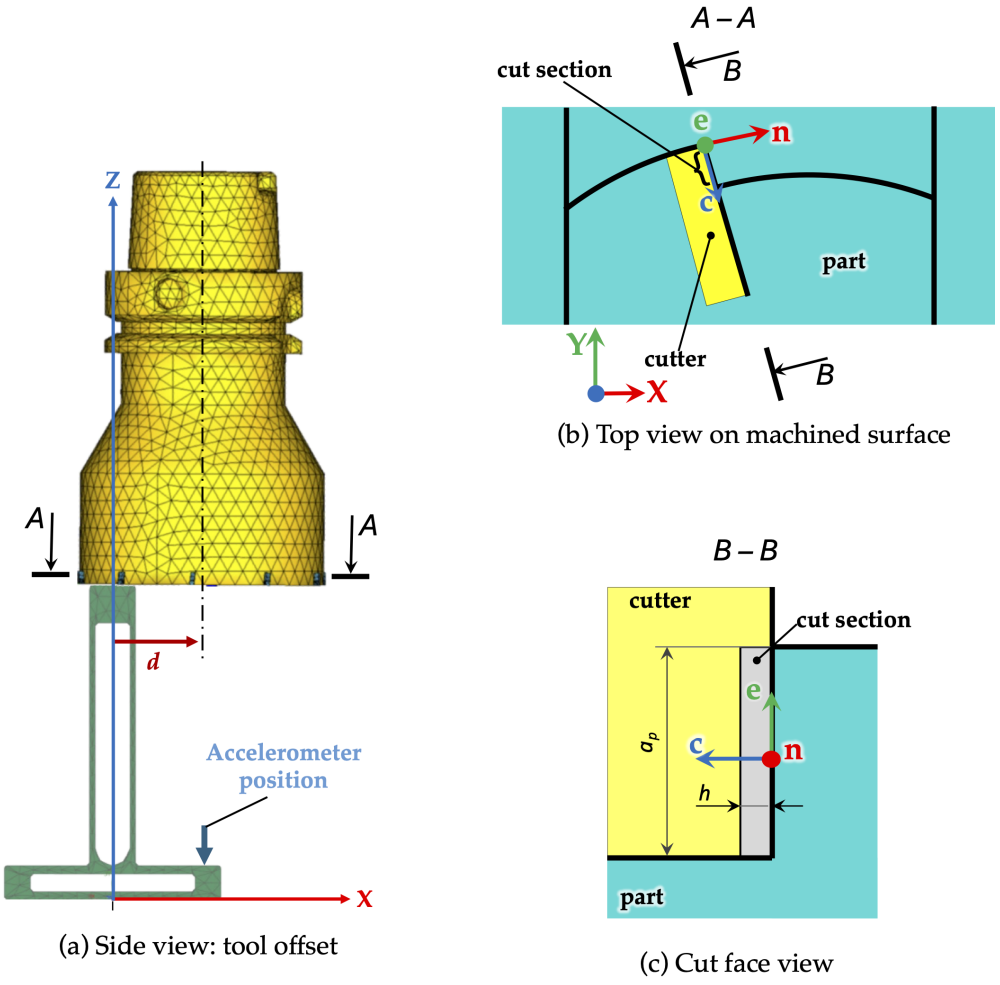

(a) Side view: tool offset

(b) Top view on machined surface

(c) Cut face view

Figure 4: Face milling operation kinematics

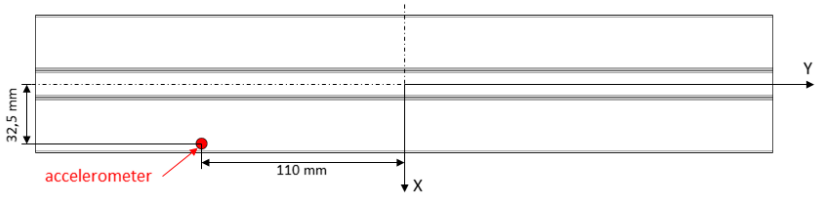

Figure 5: Accelerometer location

order evaluate time evolution of cutting forces between tool and part. This model evolves throughout the simulation and is based, in *nessy2m*, on a dexel representation [12, 19].

- A geometrical model of the teeth of the tool: needed only for the portions of the teeth that may cut the matter of the part. In *nessy2m*, each tooth is split in elementary tools in order to have a fine description of tool matter interaction (Fig. 6 shows the splitting of a tooth of the used tool). This splitting also allows a parallel approach to improve numerical efficiency. The geometry of each elementary tool is based on a B-Rep representation using a tessellation with flat triangles.

- A line force model (cutting law): used to compute components F_i of the cutting force vector $\mathbf{F}$ applied between part and tool along the tool cutting edges. These components are projections of $\mathbf{F}$ inside an orthonormal basis $(\mathbf{n}, \mathbf{e}, \mathbf{c})$ local to the cutting edge ($\mathbf{n}$ is the outward normal of the rake face, $\mathbf{e}$ is the tangent to the cutting edge and $\mathbf{c} = \mathbf{n} \times \mathbf{e}$). These directions are shown on Fig. 4b and c. An affine law $F_i(h) = K_i\, h + K_{0i}$ is used here where $i \in \{n, e, c\}$, h is the local uncut chip thickness, K_i and K_{0i} are cutting law parameters deduced from elementary tests where cutting forces are measured for different tool/part cutting conditions. A similar definition of cutting force model can be found in [20, 21].

- A dynamic model for the part, and possibly another for the tool: these models link cutting forces and vibrations/deformations of the part and the tool over time. A Finite Element (FE) eigenmodes basis are used

inside *nessy2m* for these dynamic models.

- A time integration scheme: the Newmark central differences integration scheme is used [22].

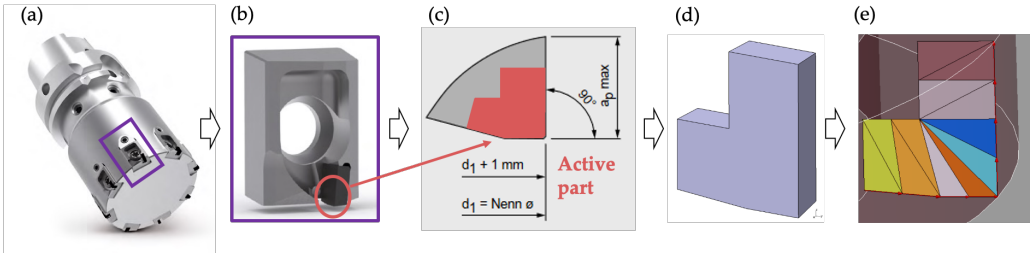

Figure 6: Geometry model of a tooth: (a) tool, (b) insert holder, (c) active part, (d) active part geometry, (e) splitting in elementary tools and associated tesselation

At the end of each time step, the matter that interacts with the volume swept by the rake faces of the tool is erased. This erasing takes into account the deformation of the part geometry generated by cutting force and dynamic effects. This makes it possible to reproduce the vibration phenomena typically encountered in machining, notably forced vibrations and regenerative chatter.

The data that can be extracted from *nessy2m* simulations can be classified in three categories:

1. quantities that can be compared to experimental measurements: surface quality represented by wavinesses and topography, acceleration/velocities/displacements during machining operation at given points of the part (depends on the nature of the used sensors),

as opposed to quantities that are not (or hardly) accessible by experimental measurements:

2. physical data used for machining behaviour analysis: cutting forces and part displacements under tool teeth,
3. purely numerical data useful to analyse the progress of an operation such as the indicator W^c proposed in Section 2.

4.3. Virtual machining model

The input dynamic model of the part is based on a set of modal shapes already used in [23]. Only the 9 first eigenmodes are retained. They are included in the range [200 Hz, 1600 Hz]. These eigenmodes are paired to experimental ones (criterion on frequency relative error under 15% and Modal Assurance Criterion (MAC) value greater than 70%). Indeed, the defects observed on flexible machined surfaces generally come from the first eigenmodes of vibrations because they contribute the most to the relative motion (displacement) of the part with respect to the tool. The shapes of these eigenmodes are given Fig. 7. One can also notice that the sensors and impacts are oriented in direction normal to the section's walls (**X** on the web and **Z** on the base), which is orthogonal to the machined surface's normal (**Z** on the web). Nonetheless, given the good correlation between FE analysis-issued modal shapes and experimental observations, and the presence of **Z** component in those shapes, the surface motion under tool is properly represented. This will also be confirmed in the following by the comparison of the machined surface profile (Fig. 8).

Experimental damping rates, noted ξ^x, and eigenfrequencies are used for the dynamic models. They are given in Tab. 2. This allows us to stay close to reality and limits the impact of the simulation model fidelity on subsequent analyses.

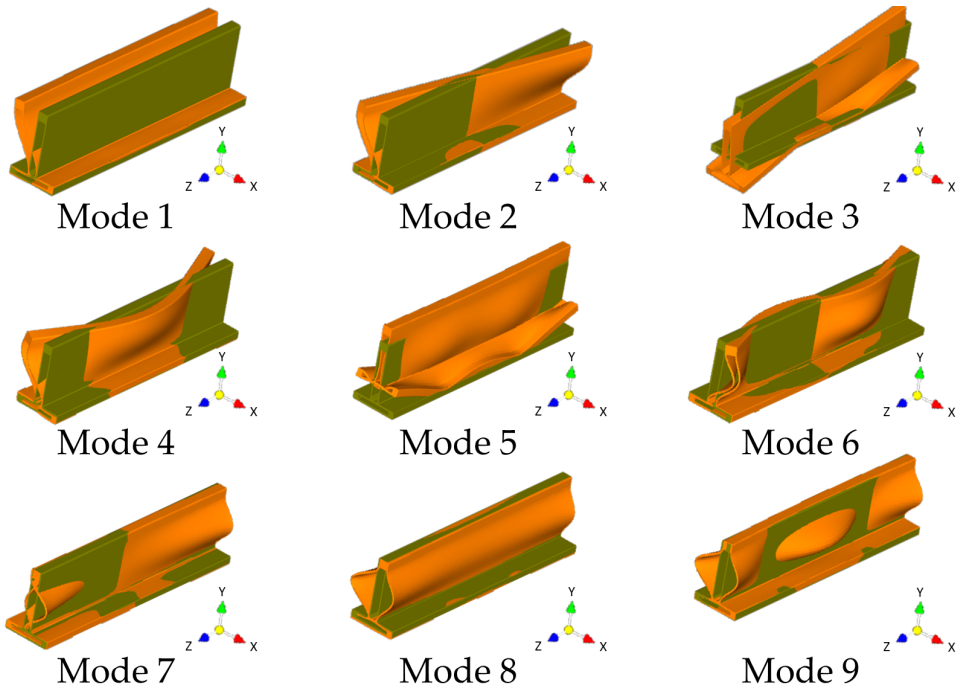

Figure 7: Shape of the first 9 eigenmodes

It should be noted that beyond 1600 Hz it was not possible to pair other numerical eigenmodes with experimental eigenmodes, given the sensor set used for modal analysis. This mainly comes from the fact that these are local eigenmodes of thin walls and the measurements carried out do not allow them to be characterized. Given that the machining occurs on a relatively massive portion of the profile and that the removed mass is negligible in comparison to the overall mass part, the modal basis is considered constant during the operation.

Considering the tool and teeth geometry, a metrology of the actual tool was carried out to obtain the difference in altitude between the teeth. This comes from an uneven axial position (along $\mathbf{Z}$) of the teeth inserts which is

adjusted within 1 μm tolerance. This was reproduced on the virtual tool to allows a detailed comparison between numerical and real machined surfaces particularly when vibrations amplitudes are smaller than 1 μm.

The used cutting law parameters K_i and K_{0i} are given in Tab. 3. These parameters were deduced from an experimental plan carried out with a dynamometric table for samples that could be considered rigid.

Eigenmode number	Exp. freq. (Hz)	Exp. damping rate ξ^x (%)
1	217.4	0.323
2	381.2	0.050
3	598.6	0.143
4	766.7	0.010
5	1145.5	0.177
6	1395.1	0.137
7	1528.0	0.327
8	1573.2	0.273
9	1634.7	0.547

Table 2: Part numerical model: eigenmodes and damping rates used for dynamic model

Finally, the width of the dexels was set to 16.67 μm and the time domain time step to $5.0 \cdot 10^{-5}$ s. These are two purely numerical parameters. The chosen dexels width corresponds to a size 3 times smaller than the feed per tooth and enables driving the equivalent cut section evaluation errors, as well as the resulting cutting forces, acceptable (below 5%). The chosen time step is 4 times smaller than the time step required by the Courant-Friedrichs-Lewy

i	n	e	c
K_i (N/mm^2)	452.43	-53.86	-265.84
K_{0i} (N/mm)	4.42	0.00	1.01

Table 3: Cutting law parameters

condition here related to the ninth eigenfrequency of 1634 Hz [22] (explicit central differences integration scheme) and leads to 12 time steps during the smallest period of the model.

4.4. Experimental versus simulation

Two tool path cases for $d = 0\,\text{mm}$ and for $d = 12.5\,\text{mm}$ are studied (see Fig. 11). The experimental measurements considered are the surface geometry and the dynamical behaviour of the part during machining operation.

Fig. 8 presents the surface topography between $Y = 45$ mm and $Y = 55$ mm. The Photography column shows pictures taken during metrological control stage. The shaded zones are not due to surface quality but to lighting system. As a confirmation, the MMT column presents an extraction of the measures performed with a chromatic white light sensor mounted on a coordinate measuring machine Zeiss O-Inspect 543. The *nessy2m* column shows extractions of the dexel surfaces coming from simulations.

The two tool paths generate quite different surfaces. For $d = 0$ mm a very regular profile is observed and corresponds to teeth passage tracks without vibrations. It can be seen, by a characteristic step in $\mathbf{Y}$ direction ($0.5\,\text{mm} = f\,Z$), that some of the teeth leave a deeper mark, likely in link with the teeth location errors discussed previously. For $d = 12.5\,\text{mm}$ the

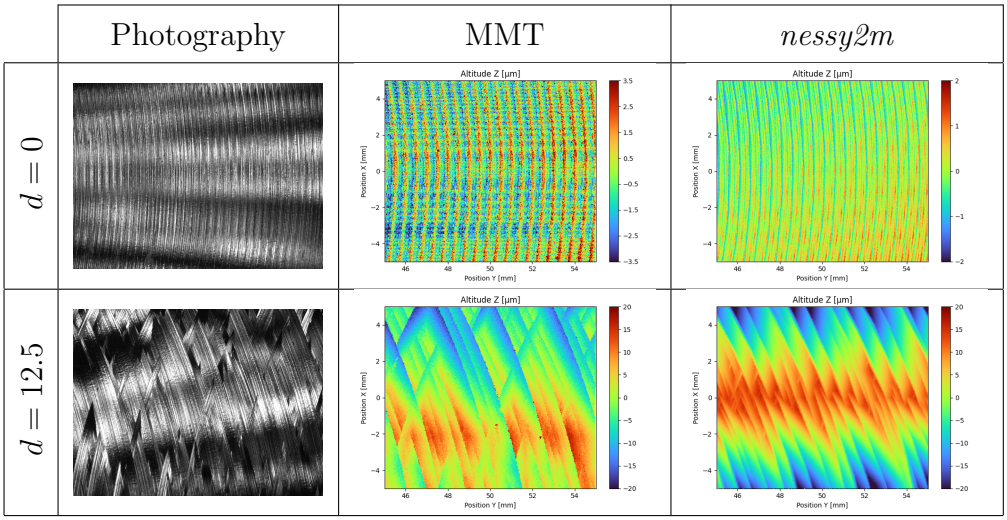

Figure 8: Surface topography: photographies, white light scanner measurements and *nessy2m* extractions

profile of the part is more bumpy and some teeth have left significantly larger marks than others. This suggests that significant vibrations appeared during this machining. This is confirmed by the analysis of the acceleration measurements. Wavinesses on both real and virtual surfaces are given in Tab. 4. The given total waviness W_t was obtained with a Gaussian filter for a cutoff length of $\lambda_c = 0.25\,\text{mm}$. The norm NF EN ISO 21920-3 indicates values of cutoff length for signal period. In our case, the Rsm value is equivalent to the feed per tooth value when no vibration occurs.

W_t [μm]	Experimental	Simulation
$d = 0$	3.6	0.6
$d = 12.5$	15.1	13.9

Table 4: Roughness values ($\lambda_c = 0.25\,\text{mm}$)

Regarding the measurement of vibrations, we extracted, from the temporal signal in acceleration, spectrograms in displacement for the 2 machining operations (Fig. 9 and Fig. 10). We have chosen to produce results in displacement because it is the history of the movements of the part at the points of contact with the teeth which defines instantaneous material removal and therefore the cutting forces which themselves generate the vibrations. In order to keep the acceleration signal within the available measurement range, the accelerometer has been placed at a small distance from a clamp. In the vicinity of clamping zones, the displacement field can be subject to systematic distortions due to unmodeled small scale boundary condition details as well as to the imperfections of the clamping model itself. Thus, the displacement magnitude comparison, especially at these low values range ($\sim 10\,\mu$m at sensors in comparison to $\sim 1\,$mm in the machined zone) can only be qualitative here. Nevertheless, spectral observations are still available in terms of matching the operation stages when specific eigenmodes are predominant in the system's vibrations.

For tool path with $d = 0\,$mm, it can be observed in the Fig. 9 that the spectral energy is well distributed on several eigenmodes for experimental measurements and simulations. No eigenmodes are predominant throughout the simulation. Naturally, eigenfrequencies of the system show a higher response especially when the tool interacts with the part. The same comment would apply for numerical simulation with generally lower amplitudes because the system considered is restricted to the machining operation itself, and would not include machine tool background noise that could induce such discrepancies. Nevertheless, these variations remain very low in abso-

lute magnitude, and one can see on the resulting surface Fig. 8 that the operation remains very close to the nominal process. This hypothesis is comforted by the second tool path case ($d = 12.5\,\text{mm}$) leading to vibrational response of the system, see Fig. 10. Their amplitudes order of magnitude are higher and so the impact of the machining center noisy environment is reduced regarding to the part dynamical response.

It can also be verified that the first eigenmodes are predominant in the system behaviour. The amplitude of each individual eigenmode does not exactly correspond between experiments and simulations. Despite these divergences it can be noticed, in accordance with Fig. 8, that the global behaviour of the machining operation is well represented.

4.5. Simulation results analysis

For the two selected tool paths, it is relatively easy to extract data from the simulations to study the acceptability of the machining operation. Indeed, for these machining operations, the tooth engagement zone is small compared to cutter's overall dimensions (the diameter of the cutter is 81 mm and the width of the machined zone is 15 mm) and at any given moment there is at most one front tooth in engagement with the material. This would not be the case if several teeth had been engaged simultaneously and if, in addition, the deformation of the part under the tool was not uniform (effect of modal shapes).

For the two trajectories, it is thus possible to examine the amplitude of matter motion under the teeth as they cut the part: displacement in the global frame at point P (see Fig. 11) positioned on the median plane of the machined surface intersecting the circle defined by the tool diameter.

For the machining operation to be considered as carried out under good conditions, these displacements must remain small compared to the feed per tooth. Moreover, it is possible to extract the contribution of each of the eigenmodes to this displacement at a given moment and at a given point on this line as it can be seen in Fig. 12 and Fig. 13. It could also be observed smooth evolution trends that can be associated to progressive evolution of part dynamics with an evolving contribution of the different eigenmodes.

For the tool paths $d = 0\,\text{mm}$ and $d = 12.5\,\text{mm}$, the major displacement is in direction **X**. This displacement component is linked to the bending of the thin walls of the part. However the displacement in **Z** direction, directly related to the final surface geometry, is considerably lower in both tool paths due to the fact that the part is stiffer in this direction (see Fig. 12 and Fig. 13 respectively). For $d = 0\,\text{mm}$ displacement **Z** direction is lower than $0.5\,\mu\text{m}$. This corresponds to the small surface defects observed on Fig. 8. For the tool path case $d = 12.5\,\text{mm}$ such a smooth evolution can not be observed and large vibrations are clearly visible. The **Z** displacements of a few tens of microns and have a significant impact on the geometry of the machined surface (see Fig. 8). For displacements according to **X**, Fig. 12 shows that eigenmodes 1 and 2, and to a lesser extent eigenmode 4, are the main contributors. One can also notice that each mode's contribution would vanish when the cutting occurs in the vicinity of nodes of respective modal shapes, such as the instants 1.4 s for mode 2 or 0.7 s for mode 4. This is consistent with the fact that the respective modal forces, modulated by the modal shapes, go through 0. It can also be observed that after the middle of the path (for $t > 2$ s), the measured response in the experiment features

a prevalent participation of mode 1 up to the end of the signal, while the simulated response in that time span predicts switching back from mode 1 to mode 2. Such difference in the high magnitude vibrations could be explained by the fact that the high magnitude interaction could potentially lead the tool-workpiece interaction out of the affine cutting law model's domain of validity. Anyway, the dominant components in the response here are systematically visible at frequencies corresponding to the respective eigenfrequencies. Furthermore, the orders of magnitude of response in $\mathbf{X}$ (strongest response, $\approx$ 1 mm) and $\mathbf{Z}$ (impact on the final surface quality, amplitude ≈ 0.010), which is consistent with the surface measurements, section 4.4.

We can now consider the computed cutting forces. The cutting forces are applied on the part by each individual elementary tool are summed and expressed in the reference frame associated to the part (see Fig. 14 where chosen instant correspond to front cutting teeth located around $Y = 50$ mm). Kinematic simulations were performed to obtain the theoretical cutting forces evolution during the milling operation with elasto-dynamics deactivated, *i.e.* in absence of workpiece and tool vibrations. These 'kinematic' cutting forces are also plotted on Fig. 14.

For $d = 0\,\text{mm}$, the activation of the dynamical behaviour of the system does not affect the cutting forces profiles: the Kinematic and Dynamic curves are superimposed. It can be deduced here that the milling process is close to the nominal milling operation. However, for $d = 12.5\,\text{mm}$, a wide variation of the cutting forces is observed. The huge values of cutting forces are explained by two main physical aspects that differ from Kinematic case. The previous analysis, based on displacements under cutting teeth extraction, has

revealed that part dynamical deflection is driven upon periods of the workpiece eigenfrequencies that are different from a tool revolution and tooth passage periods. Cutting forces generated during a portion of the tool revolution lead to a displacement pushing the part out of its nominal position. Just after this impulse the part and tool interaction is reduced. The dynamical stiffness tends to bring back the part into its original position where the teeth go back to more engaged conditions within the material. This cyclic phenomenon leads to approximately five consecutive cutting teeth interaction at relatively high force peak values, followed by non contact period of similar duration. The part global deflection during the milling operation is then generated by a sequence of strokes. In the same time the part deflection is high enough to create an interaction of the back side of the tool. Rear positioned teeth re-machined the part. It is also observed on Fig. 8 with the crossed pattern left by each individual tooth. These two physical phenomena lead to cutting engagement conditions greater than the nominal configuration, leading not only to finished surface deterioration, but also to increased risks for the tool life.

4.6. Modal work

The Fig. 15 presents the modal work summed on all eigenmodes contributions for the 2 configurations. The modal work indicator behaviour is greatly affected by vibration appearance for $d = 12.5\,\text{mm}$ with a marked difference of amplitude with respect to $d = 0\,\text{mm}$ configuration. This indicator enables to clearly discriminate the two studied configurations and their respective dynamical behaviour.

Its evolution over the tool path or the decomposition upon modal con-

tributions enable to perform a more detailed analysis about the localisation of vibration onset or also on predominant eigenmodes. One can see on Fig. 16 for $d = 12.5\,\text{mm}$ configuration that eigenmodes 1, 2 and 4 are the main contributors to W_c. More precisely, the eigenmode 2 contributes more at the start and end of the trajectory while eigenmode 1 contributes mainly at the center of the part. This is consistent with the eigenmode shapes (see Fig. 7). Fig. 16b shows Poincaré sections obtained by sampling modal work components W_{ci} with their respective frequencies ω_i. The slightly regular pattern appearing in this plot suggests that the periodicity or major components is close to respective eigenfrequencies. The smeared shape of the pattern could be caused by teeth position variance discussed in section 4.3 and the complex teeth engagement pattern shown on Fig. 14.

The strong modal response depicted above indicates the presence of self-oscillations. Nevertheless, classically invoked self-excitation mechanisms in machining would indicate such fenomena whould occur at frequencies starting at the half of the tooth passing frequency [2] which in our case would amount to 1.5 kHz), so the concrete instability mechanism leading to such response remains yet to be found.

5. Discussion

In the two studied machining configurations, the part displacement is oriented mainly along the **X** direction corresponding to the major flexibility of the part. However, the machined surface quality is mainly driven by the part displacement under cutting tool along the **Z** direction. Machined surface wavinesses, even if they highlight differences between the two surfaces, do not

provide indications about the high vibrations present during machining for the configuration $d = 12.5\,\text{mm}$.

Nevertheless, in both studied machining configurations, it is interesting to take into account the tool imperfections such as teeth altitude dispersion or the run-out of the tool. The geometrical variations of tool teeth axial location are responsible of the around 10 microns thick aspect of the displacements curves in $\mathbf{X}$ direction for the tool path configuration with $d = 0\,\text{mm}$ on Fig. 12. One can also notice on Fig. 14 a periodic variation of cutting force (synchronous with the tool rotation, at period $T = 3.33\,\text{ms}$ due to these tool imperfections. The differences between experimental and numerical surface geometry data shown on Fig. 8 could be explained by unaccounted small geometrical errors of the real machining centre and the challenging estimation of the damping rates during machining operation [24, 25] or the cutting law approximation. The milling operation dynamical behaviour is not highly affected by these aspects in our case.

Furthermore, the maximum values of the indicator W_c calculated for the tool lead to values given in Tab. 5. Despite huge cutting forces variation applied to the tool for the $d = 12.5\,\text{mm}$ configuration, the tool-related contribution to modal work (W_c tool) indicator value is greatly lower than the part-related contribution to modal work (W_c part). It indicates that the tool displacements under cutting forces are negligible in our case. It also validates the initial estimation that the part is the weakest element of this milling operation. It demonstrates the capability of the modal work indicator to guide analysis with clear identification of the more dynamically flexible component.

For configuration $d = 12.5\,\text{mm}$ it is also important to note the similarities

	max. W_c part (mJ)	max. W_c tool (mJ)
$d = 0$	0.4	1.3e-8
$d = 12.5$	216.3	1.9e-7

Table 5: Indicator W_c maximum values for the tool and the part [mJ]

between Fig. 12 and figures 15 and 16 regarding the modal contributions. These similarities show that the same indications can be deduced from part displacement in the front of the tool and modal works. This interpretation is available in our case thanks to the elongated shape of the machined portion of the workpiece along the tool trajectory. Such arrangement enables a simple definition of the tool position, point P, which nevertheless is always an approximation: the cutting interaction is distributed over finite volumes in complex motion. Moreover the analysis of the movements under the teeth is more complex when many teeth are cutting simultaneously when the width of the machined zone is of the same order of magnitude as the wavelengths of the eigenmodes. Nevertheless, the modal works are defined independently of the current position of the tool control point, on the whole interaction at each time instant, and may then be significantly easier to extract and analyse. Moreover, the observations made on the spectrograms Fig. 9 and 10 can be made based on modal works Fig. 15 and 16, given that the eigenmodes tend to exhibit high responses in the vicinity of respective eigenfrequencies. The modal works can then also be subjected to signal processing such as spectrograms or Poincaré sections. A significant difference here is the non-local nature of modal works, reflecting the whole interaction, independently of force condensation point or measurement location.

Finally, we have computed the maximum value of W_c for d variation in a wider range: $-35\,\text{mm}$ to $35\,\text{mm}$ (Fig. 17). This figure shows a very clear modification of the dynamic behaviour of the part around $d = 0\,\text{mm}$. For the surfacing of this part, the difference between conventional and climb milling his observed which is in coherence with references of the literature [4, 5]. This indicates to the user that it is very much preferable to choose a negative value for d for this operation (climb milling).

If the time evolution curves of the modal work of the cutting forces help to analyze the behavior of the machining system for a given toolpath, the comparison between these curves, and in particular here Fig. 17 relating to the comparison of the maxima of these works, allows thus to identify very effectively the differences in behavior according to the conditions of engagement of the tool.

6. Conclusion

In a process designing phase it is complex to possess a finely updated model of the studied system. Damping rates and eigenfrequencies measurements, cutting law assessment as tool run-out can not be performed and are difficult to estimate beforehand. Nevertheless numerical simulations can be a valuable means to obtain physical trends in the dynamical behaviour of a machining operation. The modal work of the cutting forces upon the part displacement is proposed as an indicator to discriminate different tool paths. Face milling operations are used to validate its relevance. After assessing the simulation fidelity regarding to machining experiments, numerical data are used to analyse the cutting forces evolution and the part displacement under

tool teeth in order to analyse vibrations. W_c trends are compared to these observations. Its maximum value is three orders of magnitude greater in our vibrated configuration as compared to the other one: from approximatively 215 mJ to 0.4 mJ. Thus the proposed indicator, using numerical extracted data, enables to guide process design by indicating the configuration leading to abnormal cutting conditions and workpiece displacements.

With the assurance of the simulation fidelity regarding to the experiment, the indicator relevancy analysis could be carried out in a process designing stage and more especially in a trajectory optimization. If the spectrograms convey similar information, the latter always depends on the location where the sensors are placed. A first essential interest of cutting modal works is that they give information directly linked to the cutting process (use of cutting forces) and to the vibrations where the tool cuts. The second interest is that it produces a synthesis (for all the teeth engaged), mode by mode, of the behaviour of the machining process whatever the complexity of the tool-material interaction. The major drawback of this descriptor is however that it is based on a simulation model which causes an implementation cost and which must also be sufficiently faithful.

References

[1] E. Budak, Y. Altintas, Analytical prediction of chatter stability in milling-parti: General formulation., J. of Dynamic Systems Measurement and Control 120 (1998) 22–30.

[2] W. T. Corpus, W. J. Endres, Added Stability Lobes in Machining Processes That Exhibit Periodic Time Variation, Part 2: Experimental

Validation, Journal of Manufacturing Science and Engineering 126 (3) (2004) 475–480, publisher: American Society of Mechanical Engineers Digital Collection. doi:10.1115/1.1765136.
URL http://asmedigitalcollection.asme.org/manufacturingscience/article/126/3/4

[3] J. Munoa, X. Beudaert, Z. Dombovari, Y. Altintas, E. Budak, C. Brecher, G. Stepan, Chatter suppression techniques in metal cutting, CIRP Annals 65 (2) (2016) 785–808. doi:10/gjhpmf.
URL https://linkinghub.elsevier.com/retrieve/pii/S0007850616301962

[4] T. Insperger, B. P. Mann, G. Stépán, P. V. Bayly, Stability of up-milling and down-milling, part 1: alternative analytical methods, International Journal of Machine Tools and Manufacture 43 (1) (2003) 25–34. doi:10/b57swc.
URL https://www.sciencedirect.com/science/article/pii/S0890695502001591

[5] C. G. Ozoegwu, S. N. Omenyi, S. M. Ofochebe, C. H. Achebe, Comparing up and down milling modes of end-milling using temporal finite element analysis, Applied Mathematics 3 (1) (2013) 1–11.

[6] L. T. Tunc, M. Zatarain, Stability optimal selection of stock shape and tool axis in finishing of thin-wall parts, CIRP Annals 68 (1) (2019) 401–404. doi:10/gr8pdh.
URL https://www.sciencedirect.com/science/article/pii/S0007850619301258

[7] L. Fan, H. Tian, L. Li, Y. Yang, N. Zhou, N. He, Machining Distortion Minimization of Monolithic Aircraft Parts Based on the Energy Principle, Metals 10 (12) (2020) 1586, number: 12 Publisher: Multidis-

ciplinary Digital Publishing Institute. doi:10.3390/met10121586.
URL https://www.mdpi.com/2075-4701/10/12/1586

[8] X. Huang, X. Liu, J. Li, Y. Chen, D. Wei, G. Ding, Machining Deformation Analysis of Aircraft Monolithic Components based on the Energy Method, Springer, 2021. doi:10.21203/rs.3.rs-182793/v2.

[9] K. Ringgaard, Y. Mohammadi, C. Merrild, O. Balling, K. Ahmadi, Optimization of material removal rate in milling of thin-walled structures using penalty cost function, International Journal of Machine Tools and Manufacture 145 (2019) 103430. doi:10/gqhw54.
URL https://www.sciencedirect.com/science/article/pii/S0890695519302421

[10] A. Gerasimenko, M. Ritou, V. Godreau, B. Furet, Monitoring of trimming operation for lightweight composite structure, Procedia CIRP 72 (2018) 1299–1304. doi:10/gr8mw6.
URL https://www.sciencedirect.com/science/article/pii/S2212827118303500

[11] M. Lamraoui, M. Thomas, M. El Badaoui, F. Girardin, Indicators for monitoring chatter in milling based on instantaneous angular speeds, Mechanical Systems and Signal Processing 44 (1) (2014) 72–85. doi:10/f5tg6m.
URL https://www.sciencedirect.com/science/article/pii/S0888327013002008

[12] S. W. Lee, A. Nestler, Virtual workpiece: Workpiece representation for material removal process, The International Journal of Advanced Manufacturing Technology 58 (Oct. 2011). doi:10.1007/s00170-011-3431-2.

[13] Y. Altintas, P. Kersting, D. Biermann, E. Budak, B. Denkena, I. Lazoglu, Virtual process systems for part machining operations, CIRP Annals 63 (2) (2014) 585–605. doi:10/f6gfnh.
URL https://www.sciencedirect.com/science/article/pii/S0007850614001899

[14] P. Lorong, G. Coffignal, E. Balmes, M. Guskov, A. Texier, Simulation of a finishing operation: milling of a turbine blade and influence of damping, in: Proceedings of ASME 2012 11th Biennal Conference on Engineering Systems design and analysis, ESDA 2012, 2012, pp. 89–98. doi:10.1115/ESDA2012-82534.

[15] M. Raffestin, Validation du dimensionnement d'opérations d'usinage de pièces industrielles sujettes à vibrations à partir de simulations, Ph.D. thesis, Ecole Nationale Supérieure d'Arts et Métiers - CER de Paris (may 2024).

[16] G. V. D. Roches, E. Balmès, Understanding friction induced damping in bolted assemblies through explicit transient simulation, in: International Conference on Noise and Vibration Engineering, KUL, 2014, pp. ID–360.
URL https://hal.science/hal-01066967

[17] Y. Yang, L. Fan, L. Li, G. Zhao, N. Han, X. Li, H. Tian, N. He, Energy principle and material removal sequence optimization method in machining of aircraft monolithic parts, Chinese Journal of Aeronautics 33 (10) (2020) 2770–2781. doi:10.1016/j.cja.2020.05.018.
URL https://www.sciencedirect.com/science/article/pii/S1000936120302430

[18] G. Coffignal, P. Lorong, L. Illoul, A general method to accurately simu-

late material removal in virtual machining of flexible workpieces, Internal Report (2015).
URL https://hal.archives-ouvertes.fr/hal-03184509/document

[19] V. Dambly, É. Rivière-Lorphèvre, O. Verlinden, Tri-dexel based cutter-workpiece engagement determination for robotic machining simulator, Procedia CIRP 107 (2023) 1059–1064. doi:10.1016/j.procir.2022.05.108.
URL https://linkinghub.elsevier.com/retrieve/pii/S2212827122003924

[20] M. Salehi, T. L. Schmitz, R. Copenhaver, R. Haas, J. Ovtcharova, Probabilistic Prediction of Cutting and Ploughing Forces using Extended Kienzle Force Model in Orthogonal Turning Process, Procedia CIRP 77 (2018) 90–93. doi:10.1016/j.procir.2018.08.228.
URL https://www.sciencedirect.com/science/article/pii/S2212827118310771

[21] A. Gerasimenko, M. Guskov, J. Duchemin, P. Lorong, A. Gouskov, Variable Compliance-related Aspects of Chatter in Turning Thin-walled Tubular Parts, Procedia CIRP 31 (2015) 58–63. doi:10.1016/j.procir.2015.03.088.

[22] M. Géradin, D. J. Rixen, Mechanical vibrations: theory and application to structural dynamics, John Wiley & Sons, 2014.

[23] M. Raffestin, C. Urville, P. Lorong, M. Guskov, Battery Tray Fixture Stiffness and Damping Modeling for Surface Quality Prediction, Procedia CIRP 117 (2023) 145–150. doi:10/gr639k.
URL https://www.sciencedirect.com/science/article/pii/S2212827123001580

[24] Y.-Y. Ren, M. Wan, W.-H. Zhang, Y. Yang, A review on methods for obtaining dynamical property parameters of machining processes, Mechanical Systems and Signal Processing 194 (2023) 110280. doi:10.1016/j.ymssp.2023.110280.
URL https://linkinghub.elsevier.com/retrieve/pii/S0888327023001875

[25] A. Iglesias, L. Taner Tunç, O. Özsahin, O. Franco, J. Munoa, E. Budak, Alternative experimental methods for machine tool dynamics identification: A review, Mechanical Systems and Signal Processing 170 (2022) 108837. doi:10.1016/j.ymssp.2022.108837.
URL https://linkinghub.elsevier.com/retrieve/pii/S0888327022000346

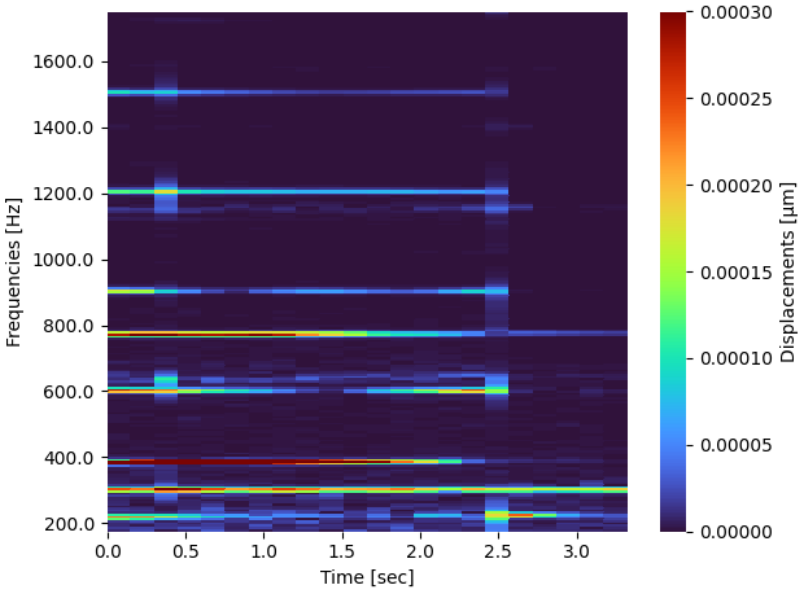

(a) Experimental measurement spectrogram

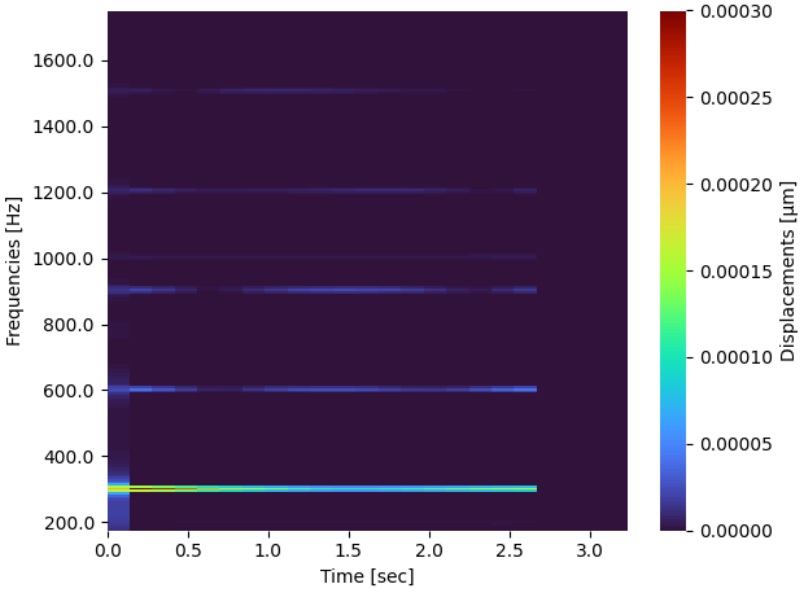

(b) Numerical simulation spectrogram

Figure 9: Configuration $d = 0\,\text{mm}$ - Spectrograms

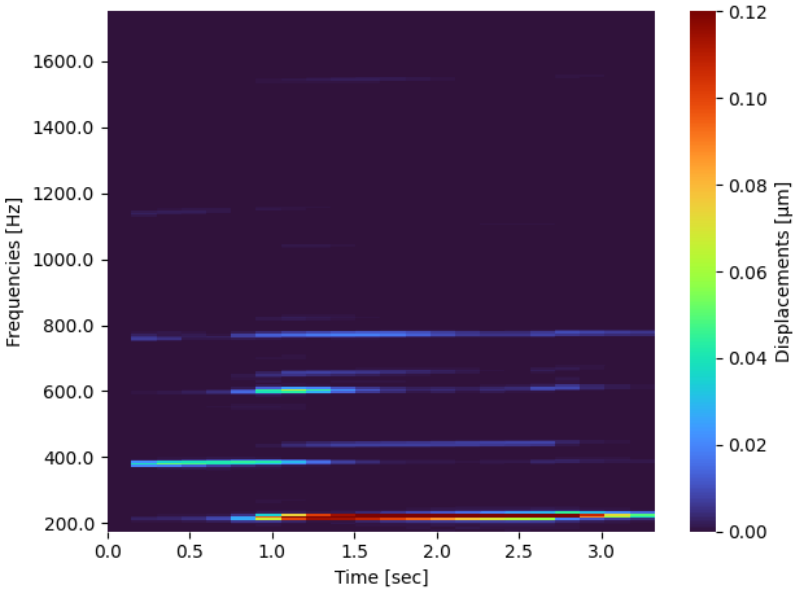

(a) Experimental measurement spectrogram

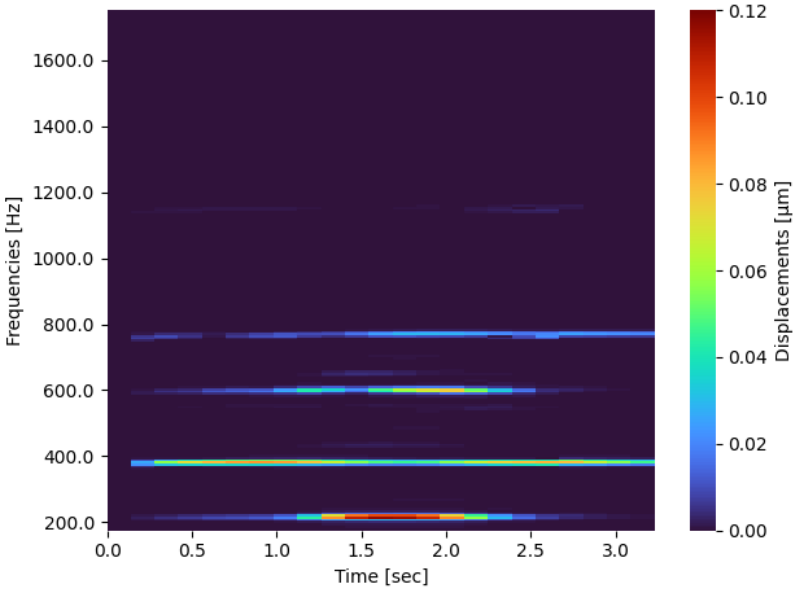

(b) Numerical simulation spectrogram

Figure 10: Configuration $d = 12.5\,\text{mm}$ - Spectrograms

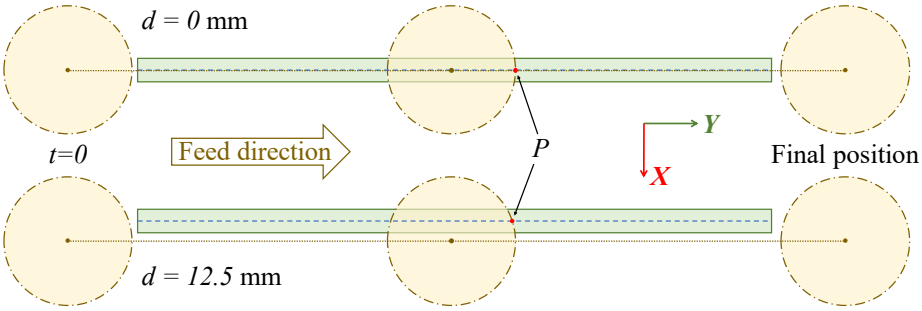

Figure 11: Location of measurement point P for displacement under teeth

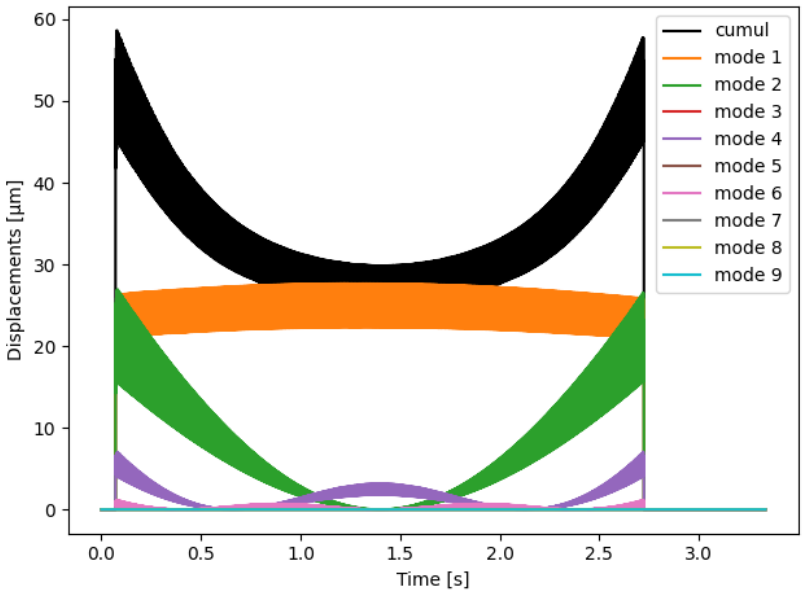

(a) Configuration $d = 0\,\text{mm}$

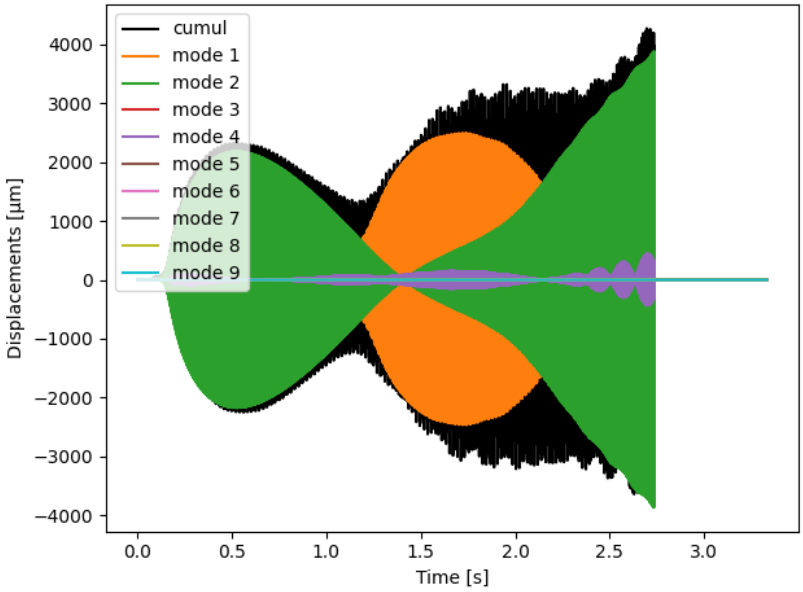

(b) Configuration $d = 12.5\,\text{mm}$

Figure 12: Modal contributions on part displacement at P: direction **X**

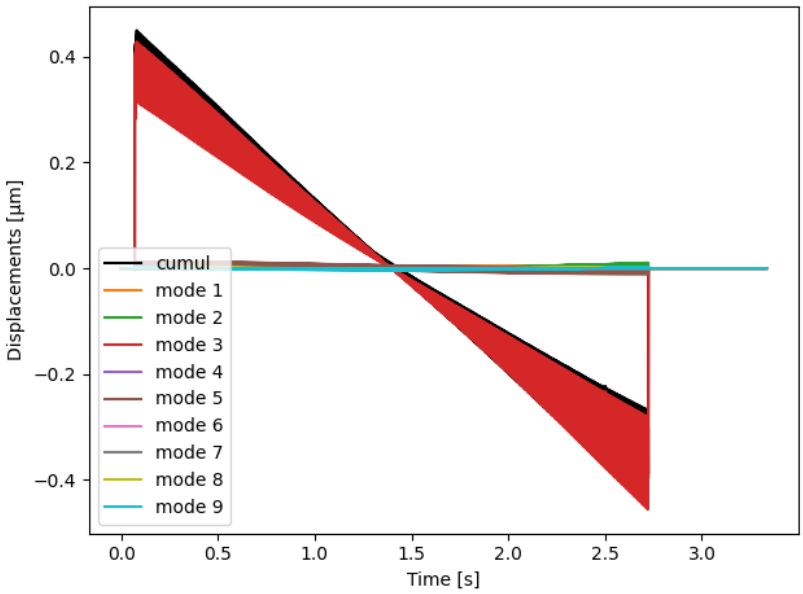

(a) Configuration $d = 0\,\text{mm}$

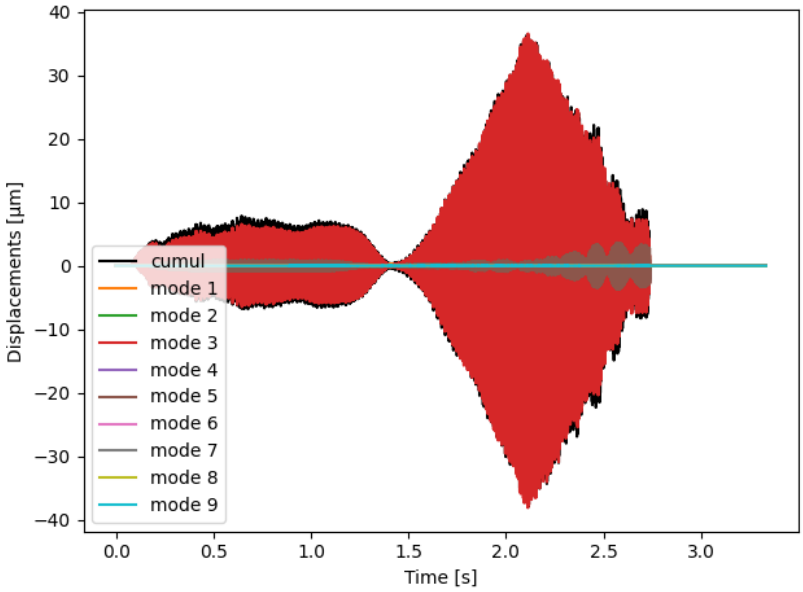

(b) Configuration $d = 12.5\,\text{mm}$

Figure 13: Modal contributions on part displacement at P: direction **Z**

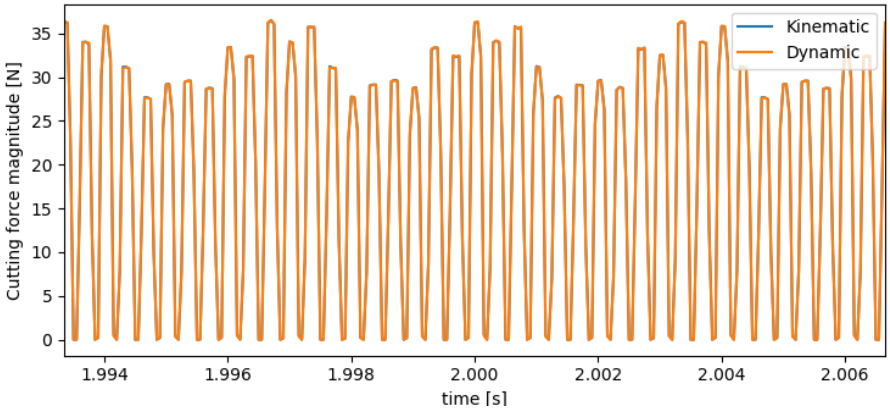

(a) Configuration $d = 0$ mm

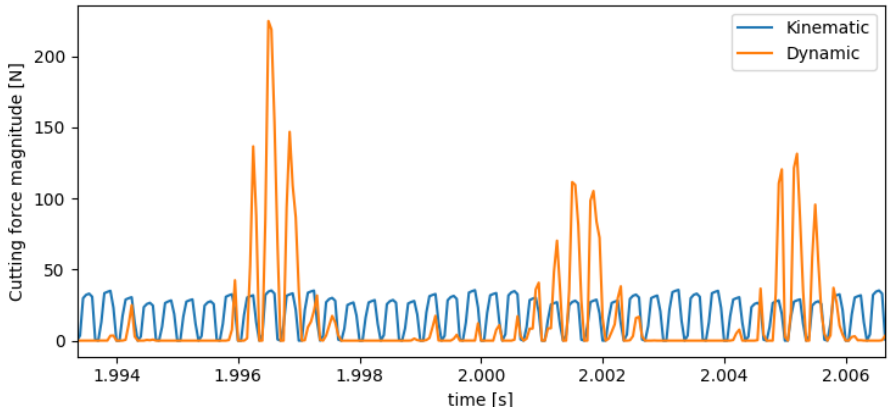

(b) Configuration $d = 12.5$ mm

Figure 14: Evolution of cutting force modulus

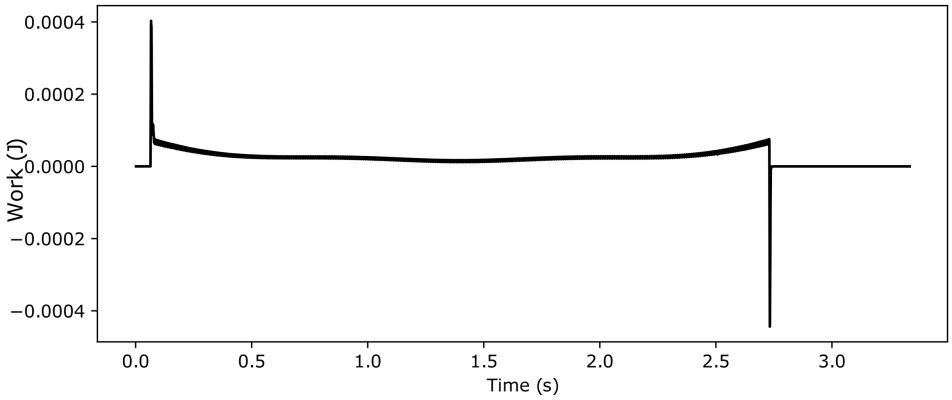

(a) Configuration $d = 0\,\text{mm}$

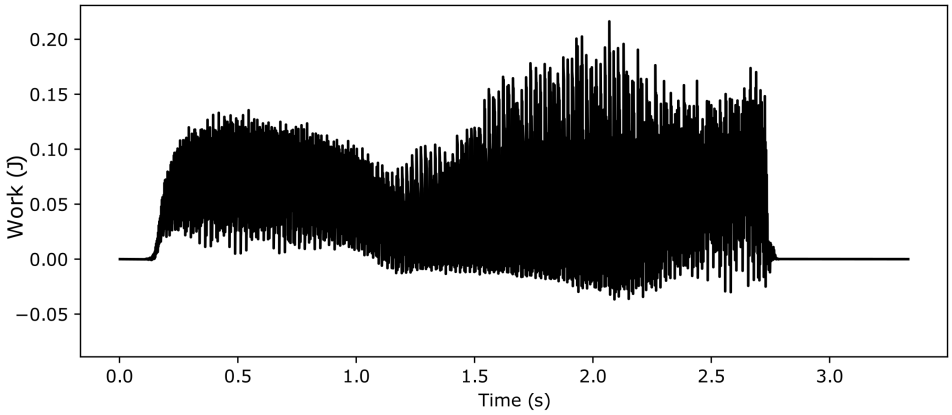

(b) Configuration $d = 12.5\,\text{mm}$

Figure 15: W_c evolution graphs

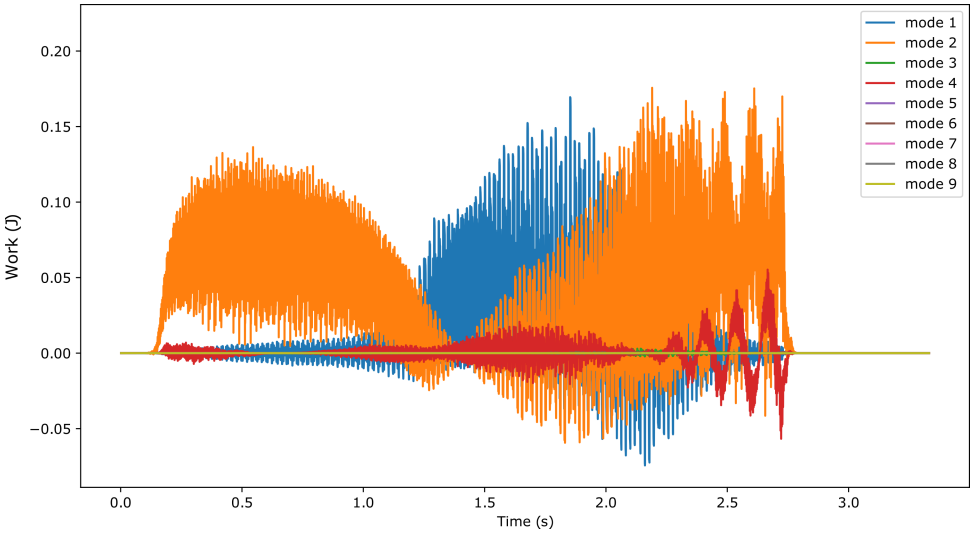

(a) $W_{ci}(t, T)$

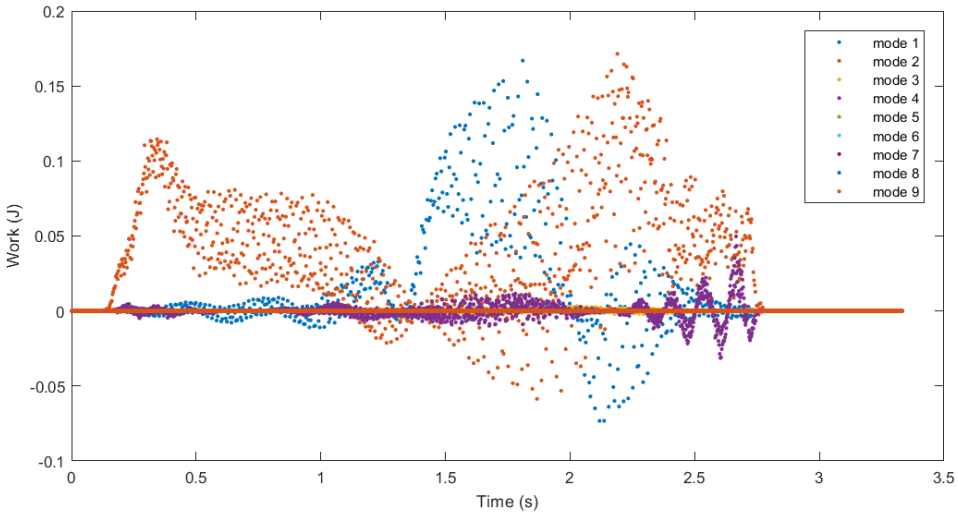

(b) $W_{ci}(t, T)$ sampled with respective modal periods $T_i = \frac{2\pi}{\omega_i}$

Figure 16: Evolution of eigenmodes contributions to W_{ci}, configuration $d = 12.5\,\text{mm}$

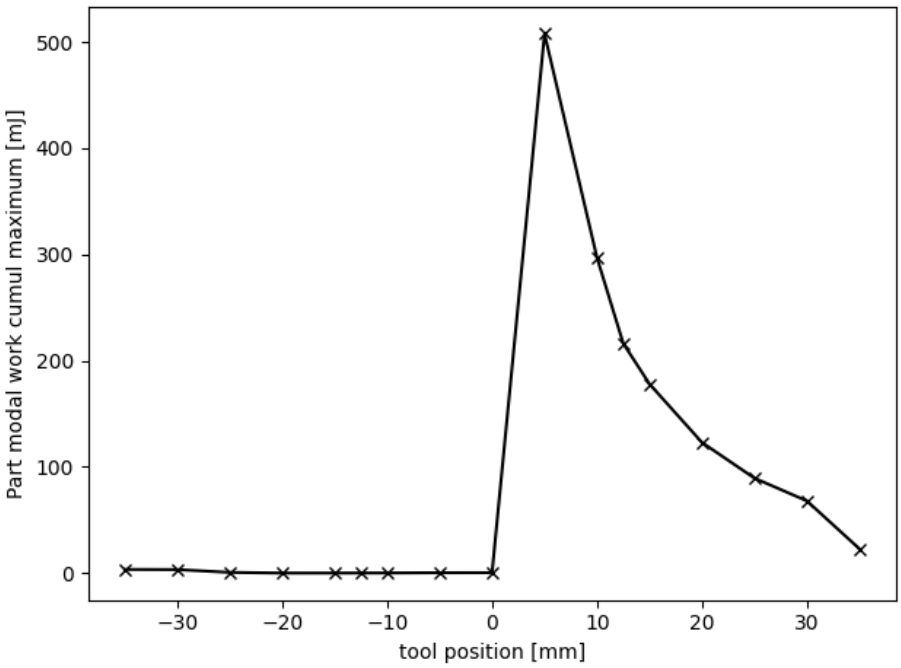

Figure 17: Evolution of maximum value of W_c for $d \in [-35., 35.]$ mm